SUPPLEMENTARY INFORMATION

FIGURES
DR1-DR7

MATERIAL AND METHODS

Description of the Drilling site

In May 2016 the joint program of the International Ocean Discovery Program (IODP) and the Continental Drilling Program (ICDP) Expedition 364 drilled the Chicxulub crater at the peak ring. The drill site MOO77A was located offshore the Yucatan Peninsula, Mexico (21.45º N, 89.95º W) (Gulick et al., 2017).

Open hole drilling occurred from the seabed (19.8 m) to ~500 meters below sea floor (mbsf). Core material was recovered between 505.7 and 1334.7 mbsf. The post impact sedimentary rock was recovered between 505.70–617.28 mbsf containing a diverse suite of lithologies (such as claystone, black shale, marlstone, siltstone and limestones). The core material from the upper peak ring (617.33 - 747.02 mbsf was composed of suevite overlaying clast-poor impact melt rock. The lower peak ring (747.02 – 1334.69 mbsf) is characterised by shocked granitoids intruded by pre-impact dikes as well as suevite and impact melt rock. The K/Pg boundary separates the post-impact sediments from the upper peak ring (617.28 and 617.33 mbsf) (Gulick et al., 2017; Morgan et al., 2016; Gulick et al., 2019) see also IODP website for Expedition 364) (https://doi.org/10.14379/iodp.proc.364.2017).

Extraction of sediments and fractionation

The core samples (up to 20 g) were surface cleaned by ultra-sonication in milli-Q water (2x for 15 min) to remove any remaining water-soluble drilling fluids. Thereafter, the samples were freeze-dried and then surface cleaned for any solvent soluble contaminants using an

ultrasonic bath (3x for 15 min in a solvent mixture of dichloromethane (DCM) and methanol (MeOH), 9:1 vol./vol.). The dried samples were ground using a pestle and mortar and Soxhlet extracted (72 h using a solvent mixture of DCM:MeOH, 9:1 vol./vol.). The extracts were passed through a Pasteur pipette filled with activated copper powder to remove elemental sulfur. Excess solvent was carefully removed under a gentle stream of nitrogen and the extracts weighed.

The weighed extracts were fractionated by small-scale column liquid chromatography. The sample (up to 10 mg) was applied to the top of a small column (5 cm × 0.5 cm i.d.) of activated silica gel (150 °C, 8 h) preconditioned with n-hexane. The saturated hydrocarbon fraction was eluted with n-hexane (4 mL), the aromatic hydrocarbon fraction with n-hexane and dichloromethane (4 mL, 9:1 vol./vol.), and the polar fraction with a mixture of dichloromethane and methanol (4 mL, 1:1 vol./vol.). For samples 616.26 – 617.26 mbsf please see below.

Samples 616.26 – 617.26 mbsf: Analysis of saturated fraction of the transitional layer: Samples were freeze dried and powdered prior to lipid extraction and fractionation as per Magill et al., 2015

Analyses

Gas Chromatography-Mass Spectrometry (GC-MS)

The saturated and aromatic hydrocarbon fractions were analyzed by gas chromatography mass spectrometry (GC–MS). The analyses were performed using an Agilent 5975B MSD interfaced to an Agilent 6890 gas chromatograph, which was fitted with a DB-1MS UI capillary column for saturated fractions and a DB-5MS UI capillary column for aromatic fractions (both columns J and W Scientific, 60 m, 0.25 mm i. d., 0.25 μm film thickness). Samples were dissolved in n-hexane and injected on-column using an Agilent 7683B auto-sampler. The GC oven was ramped from 40 °C to 325 °C at a heating rate of 3 °C/min with initial and final hold times of 1 and 30 min, respectively. Helium was used as carrier gas at a constant flow of 1.1 ml/min. The MS was operating with a standardized ionization energy of 70 eV, a source temperature of 230 °C and an electron multiplier voltage of 1706 V, scanning a mass range of 50–550 Daltons (2.91 scans per second). Saturated and aromatic hydrocarbons were identified by comparison of mass spectra and by matching retention times with those of reference compounds reported previously (Grice et al. 2007, 1996).

Samples 616.26 – 617.26 mbsf: The aliphatic fraction was analyzed by GC-MS (Agilent 7890A GC coupled to a mass selective detector 5975 MSD) in full scan mode for compound identification and in selective ion monitoring mode (ions 191, 205, 217, 218) for measurement.

Gas Chromatography-Triple Quad- Mass Spectrometry (GC-QQQ_MS)

The saturated and aromatic fraction were combined and analyzed by GC-QQQ-MS for carotenoids, hopanes, steranes and their methylated derivatives (French et al. 2015), using an Agilent 7890B GC coupled with an Agilent 7010B Triple Quadruple MS operated in multiple reaction monitoring (MRM) mode. The gas chromatograph was fitted with a DB-5MS UI capillary column (Agilent 122-5562 UI, 60 m, 0.25 mm i. d., 0.25 μm film thickness). Helium was used as carrier gas (constant flow 1.1747 ml/min). The GC oven was ramped from 40°C to 325°C at a heating rate of 4°C/min with a holding time of 20.75 min at 325°C. The MS was operating with an ionization energy of 50 eV and source temperature of 250ºC. The temperature of the QQQ was 150ºC. The collision energy for all compounds was 5 eV except for the carotenoids (10 eV). The following transitions were monitored m/z 370 → 191 (C_{27} hopanes), m/z 384 → 191 (C_{28} hopanes), m/z 398 → 191 (C_{29} hopanes), m/z 412 → 191 (C_{30} hopanes), m/z 426 → 191 (C_{31} hopanes), m/z 440 → 191 (C_{32} hopanes), m/z 454 → 191 (C_{33} hopanes), m/z 468 → 191 (C_{34} hopanes), m/z 482 → 191 (C_{35} hopanes), m/z 426 → 205 (C_{31} methylhopanes), m/z 358 → 217 (C_{26} steranes), m/z 372 → 217 (C_{27} steranes), m/z 386 → 217 (C_{28} steranes), m/z 400 → 217 (C_{29} steranes), m/z 414 → 217 (C_{30} steranes), m/z 414 → 98 (dinosteranes), m/z 558 → 123 (β-carotane), m/z 554 → 134 (chlorobactene & okenane) m/z 552 → 134 (β-isorenieratane), m/z 546 → 134 (isorenieratane), m/z 376.3 → 221(D4-C_{27} ααα cholestane). D4-C_{27} ααα cholestane was added as an internal standard. The analytes were identified by comparison with reference standards, matching retention times and elution order.

Samples 616.26 – 617.26 mbsf: Only the aliphatic fraction was analysed.

Heterocyst glycolipid analysis

An aliquot of each polar fraction was dissolved in a mixture of n-hexane:2-propanol:H_2O (72:27:1, vol./vol./vol.) to a concentration of 10 mg/ml and subjected to heterocyst glycolipid (HG) analysis as described by Bauersachs et al., (2015). Separation of HGs was achieved

using a Waters Alliance 2690 HPLC system equipped with a Phenomenex Luna NH$_2$ column (150×2 mm; 3 μm particle size) and a guard column of the same material, which were both maintained at 30°C. Heterocyst glycolipids were eluted using the following gradient profile: 95% A/5% B to 85% A/15% B in 10 min (held 7 min) at 0.5 mL/min, followed by back flushing with 30% A/70% B at 0.2 mg/mL for 25 min and re-equilibrating the column with 95% A/5% B for 15 min. Solvent A was n-hexane:2-propanol:HCO$_2$H:14.8 M NH$_3$ aq. (79:20:0.12:0.04; vol./vol./vol./vol.) and solvent B was 2-propanol:water:HCO$_2$H:14.8 M NH$_3$ aq. (88:10:0.12:0.04; vol./vol./vol./vol.).

Detection of HGs was performed using a Micromass Quattro LC triple quadrupole MS equipped with an electrospray ionization (ESI) interface and operated in positive ion mode. Source conditions were as follows: capillary 3.5 kV, cone 20 V, desolvation temperature 230°C, source 120°C; cone gas 80 L/h and desolvation gas 230 L/h. HGs were recorded in MRM mode using previously established mass spectral information (Bauersachs et al., 2009,2013; Wömer et al. 2012; Schouten et al., 2013; Bale et al., 2013) and monitoring the following transitions: m/z 547 → 415 (pentose HG$_{26}$ diol), m/z 561 → 415 (deoxyhexose HG$_{26}$ diol), m/z 575 → 413 (HG$_{26}$ keto-ol), m/z 577→ 415 (HG$_{26}$ diol), m/z 603 → 471 (pentose HG$_{30}$ diol), m/z 603 → 441 (HG$_{28}$ keto-ol), m/z 605 → 443 (HG$_{28}$ diol), m/z 619 → 487 (pentose HG$_{30}$ triol), m/z 619 → 457 (HG$_{28}$ keto-diol), m/z 621 → 459 (HG$_{28}$ triol), m/z 631 → 469 (HG$_{30}$ keto-ol), m/z 633 → 471 (HG$_{30}$ diol), m/z 635 → 459 (methyl-C$_6$ HG$_{28}$ triol), m/z 647 → 515 (pentose HG$_{32}$ triol), m/z 647 → 485 (HG$_{30}$ keto-diol), m/z 649 → 483 (HG$_{30}$ triol), m/z 675 → 513 (HG$_{32}$ keto-diol) and m/z 677 → 515 (HG$_{32}$ triol). As no authentic HG standards are commercially available, here we semi-quantified HGs as the integrated peak area counts (a.c.)/gram TOC. Fractional abundances of each HG were obtained by normalizing peak areas to the summed area of all 18 HGs included in the MRM method.

Total organic carbon

The rock samples were ground to a fine powder and digested in acid (HCl) to remove the carbonate minerals. The remaining samples were analysed using a LECO Carbon-Sulfur Analyser (CS-230). The CO$_2$ produced was measured with an infra-red detector, and values calculated according to standard calibration.

TOC in samples

The total organic carbon (TOC) in the entire interval studied was low, ranging between 0.06 to 0.2 wt . It appears that in certain intervals the the *n*-alkanes ratios mirror the TOC concentration suggesting that the low TOC might be the driver of the pattern. Statistical analyses of long chain alkanes n-C_{25}-C_{35} vs TOC values showed no correlations, apart from the transitional unit and white micrite (grey section Fig. 2A) which showed a significant negative correlation with a P value of 0.0039 at a significance level $p < 0.05$ (N = 16). Below and above the transitional unit no correlation was found. We conclude from this that the TOC was not the main driver of the long chain *n*-alkane distribution (Figure S7)

Carbon isotopes

For the bulk stable carbon isotope compositions ($^{13}C/^{12}C$) the extracted samples were digested in 1M HCl to remove carbonate minerals. The bulk $\delta^{13}C$ analysis was performed using a Thermo Flash 2000 HT elemental analyser (EA) connected to a Delta V Advantage isotope ratio mass spectrometer (irMS) *via* a Conflo IV. Samples were weighed (~2 mg) in triplicate into tin cups (SerCon) and combusted to CO_2 in the nitrogen-carbon reactor (1020 °C). CO_2 passed through the Conflo IV interface into the irMS, which measured *m/z* 44, 45 and 46. $\delta^{13}C$ values were calculated by Thermo Isodat software and normalised to the international VPDB scale by multi-point normalisation using the standard reference materials NBS 19 (+1.95 ‰) and L-SVEC (-46.6 ‰) (Coplen *et al*., 2006). The standard reference material IAEA-600 was measured during the sequence to evaluate the accuracy of the normalisation. The normalised $\delta^{13}C$ values of IAEA-600 from these measurements were within ± 0.1 ‰ of the reported value of -27.77 ‰ (Coplen et al., 2006).

Sulfur isotopes of reduced sulfur

The sulfur isotope composition ($^{34}S/^{32}S$) of total reduced inorganic sulfur (TRIS; considered to represent pyrite (FeS_2)) was extracted from ground sediments via hot acidic chromium (II) chloride distillation following Fossing and Jørgensen, (1989). The generated hydrogen sulfide (H_2S) was transported in a stream of N_2 through a Zn acetate solution trap and precipitated quantitatively as ZnS. Sulfide concentrations were measured spectrophotometrically by the methylene blue method (Cline, 1969) and converted to solid phase contents. For isotope measurements, the trapped ZnS was transformed to Ag_2S with a 1 M $AgNO_3$ solution, washed and dried. The sulfur isotopic composition was measured by combustion-isotope ratio monitoring mass spectrometry (C-irmMS) using a Thermo Scientific IsoLink elemental

analyser coupled to a Thermo Finnigan MAT 253 mass spectrometer via a Thermo Scientific Conflo IV interface. Mass spectrometric results were calibrated to the V-CDT scale using IAEA isotope reference materials following Mann et al., (2009).

REFERENCES CITED

Bale, N.J., Hopmans, E.C., Dorhout, D., Stal, L.J., Grego, M., van Bleijswijk, J., Sinninghe Damsté, J.S., and Schouten, S., 2018, A novel heterocyst glycolipid detected in a pelagic N2 -fixing cyanobacterium of the genus Calothrix: Organic Geochemistry, v. 123, p. 44-47, https://doi.org/10.1016/j.orggeochem.2018.06.009.

Bauersachs, T., Hopmans, E.C., Compaoré, J., Stal, L.J., Schouten, S., and Sinninghe Damsté, J. S., 2009, Rapid analysis of long-chain glycolipids in heterocystous cyanobacteria using high-performance liquid chromatography coupled to electrospray ionization tandem mass spectrometry: Rapid Communications in Mass Spectrometry, v. 23, p. 1387-1394, https://doi:10.1002/rcm.4009.

Bauersachs, T., Rochelmeier, J., and Schwark, L., 2015, Seasonal lake surface water temperature trends reflected by heterocyst glycolipid-based molecular thermometers: Biogeosciences, v. 12, p. 3741-3751, https://doi:10.5194/bg-12-3741-2015.

Bauersachs, T., T., Miller, S.R., van der Meer, M.T.J., Hopmans, E.C., Schouten, S., and Sinninghe Damsté, J.S., 2013, Distribution of long chain heterocyst glycolipids in cultures of the thermophilic cyanobacterium Mastigocladus laminosus and a hot spring microbial mat: Organic Geochemistry, v. 56, p. 19-24, https://doi:10.1016/j.orggeochem.2012.11.013.

Cline, J.D., 1969, Spectrophotometric Determination of Hydrogen Sulfide in Natural Waters: Limnology and Oceanography, v. 14, p. 454-458, https://doi:10.4319/lo.1969.14.3.0454.

Coplen, T.B., Brand, W.A., Gehre, M., Gröning, M., Meijer, H.A.J., Toman, B., Verkouteren, R.M., 2006, New Guidelines for δ^{13}C Measurements: Analytical Chemistry, 78(7), 2439-2441. https://doi.org/10.1021/ac052027c.

Fossing, H. and Jørgensen, B.B., 1989, Measurement of bacterial sulfate reduction in sediments: evaluation of a single-step chromium reduction method: Biogeochemistry, v. 8, p. 205–222, https://doi:10.1007/BF00002889.

French, K. L., Rocher, D., Zumberge, J. E. and Summons, R. E., 2015, Assessing the distribution of sedimentary C40 carotenoids through time: Geobiology, v. 13, p. 139-151. https://doi:10.1111/gbi.12126.

Grice, K., Nabbefeld, B., and Maslen, E., 2007, Source and significance of selected polycyclic aromatic hydrocarbons in sediments (Hovea-3 well, Perth Basin, Western Australia) spanning the Permian–Triassic boundary: Organic Geochemistry, v. 38, p. 1795-1803, https://doi:10.1016/j.orggeochem.2007.07.001.

Grice, K., Schaeffer, P., Schwark, L., and Maxwell, J.R., 1996, Molecular indicators of palaeoenvironmental conditions in an immature Permian shale (Kupferschiefer, Lower Rhine Basin, north-west Germany) from free and S-bound lipids: Organic Geochemistry, **25**, 131-147, https://doi:10.1016/S0146-6380(96)00130-1..

Gulick, S. et al., 2017, Chicxulub: Drilling the K-Pg Impact Crater. Proceedings of the International Ocean Discovery Program, 364: College Station, TX (International Ocean Discovery.Program). https://doi.org/10.14379/iodp.proc.364.101.2017.

Gulick, S. et al., 2019, The first day of the Cenozoic: Proceedings of the National Academy of Sciences of the United States of America, v. 116, 19342-19351, https://doi:10.1073/pnas.1909479116.

Magill, C.R., Denis, E.H., and Freeman, K.H., 2015, Rapid sequential separation of sedimentary lipid biomarkers via selective accelerated solvent extraction: Organic Geochemistry, v. 88, p. 29-34, https://doi:10.1016/j.orggeochem.2015.07.009.

Mann, J.L., Vocke, R.D., and Kelly, W.R., 2009, Revised $\delta^{34}S$ reference values for IAEA sulfur isotope reference materials S-2 and S-3: Rapid communications in Mass Spectrometry, v. 23, p. 1116-1124. https://doi:10.1002/rcm.3977.

Morgan J.V. et al., 2016, The formation of peak rings in large impact craters: Science, v. 354, p. 878-882, https://doi:1095-9203.

Schouten, S., Villareal, T.A., Hopmans, E.C., Mets, A., Swanson, K.M., and Sinninghe Damsté, J.S., 2013, Endosymbiotic heterocystous cyanobacteria synthesize different heterocyst glycolipids than free-living heterocystous cyanobacteria: Phytochemistry, v. 85, p. 115-121, https://doi:10.1016/j.phytochem.2012.09.002.

Wörmer, L., Cirés, S., Velázquez, D., Quesada, A., and Hinrichs, K.U., 2012, Cyanobacterial heterocyst glycolipids in cultures and environmental samples: Diversity and biomarker potential: Limnology and Oceanography, v.57, p. 1775-1788, https://doi:10.4319/lo.2012.57.6.1775.
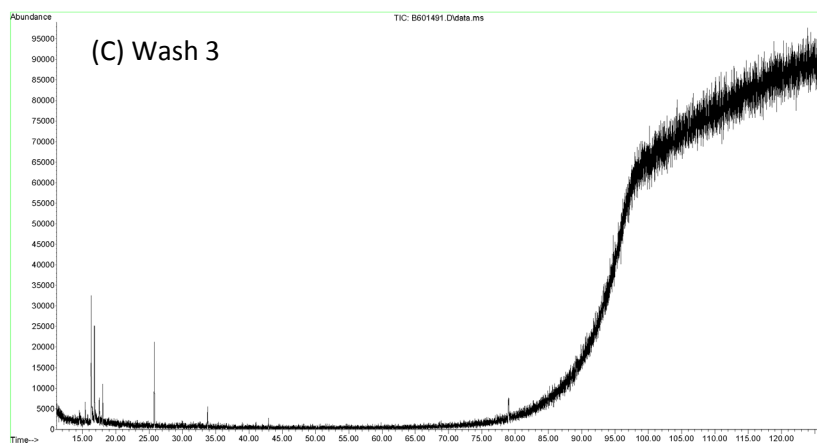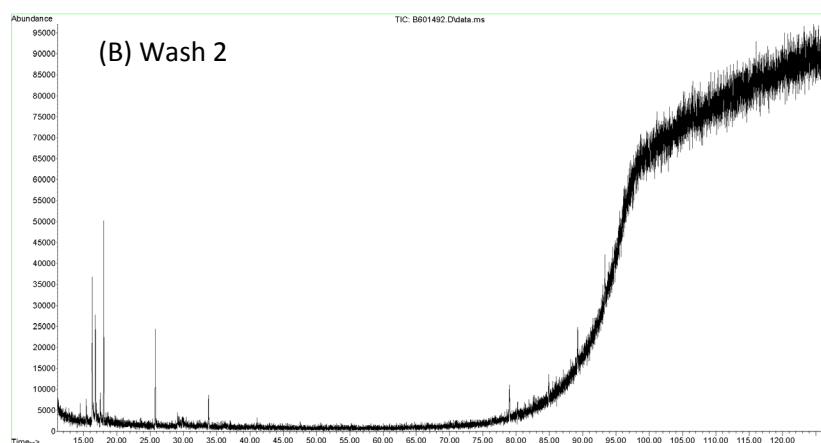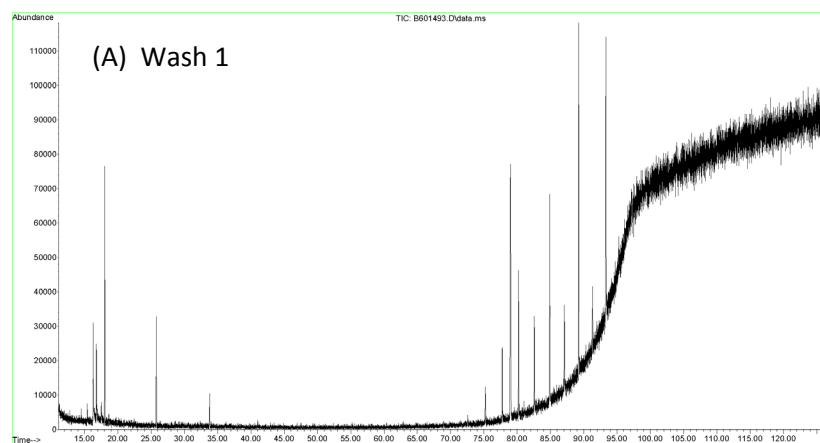
Figure Captions DR1- DR7

Figure DR1. Example of GC-MS chromatographs of a limestone sample surface cleaned. Samples were sonicated 3x for 15 min in a solvent mixture of dichloromethane (DCM) and methanol (MeOH), 9:1 vol./vol.).

 (A) Wash 1

 (B) Wash 2

 (C) Wash 3

Figure DR2. GC-MS chromatograms of a procedural blank. Empty thimble Soxhlet extracted 72 h using a solvent mixture of DCM:MeOH, 9:1 (vol./vol.).

Figure DR3. MRM chromatograms of procedural blank (showing for carotenoids). Empty thimble Soxhlet extracted for 72 h using a solvent mixture of DCM:MeOH, 9:1 (vol./vol.).

Figure DR4. MRM-Chromatograms for carotenoids in a sample of the limestone interval at the depth of 613.12 mbsf. S/N: signal to noise ratio.

Figure DR5. Ts/(Ts+Tm) and homophopane 22*S*/(22*S* + 22*R*) ratios. The ratios are 0.6 or below supporting low thermal maturity (Peters and Moldowan, 1991). (Ts (18α-22, 29, 30-trisnorneohopane), Tm (17α-22, 29, 30-trisnorhopane).

Figure DR6. Fractional abundance of heterocyst glycolipids. Fractional abundance of HGs derived from N_2-fixing filamentous heterocysts in extractable lipids against the lithology of the Chicxulub core (Yucatán Peninsula, México) from IODP Site M0077A. Compounds were identified by mass spectral characteristics (see supplementary text for analyses). HG_{26} diol and keto-ol are the most commonly HGs found in the post-impact sediments only in the limestone interval HG_{30} and HG_{32} triol occur, indicating a shift in the cyanobacterial community. The heterocystous cyanobacteria and the Chlorobiaceae and Chromatiaceae biomarkers shown in Figure 4 support a common microbial mat origin at ~ 613 mbsf (~1 Ma after impact).

Figure DR7. Long chain n-alkanes C_{25} – C_{33} vs TOC. Significant negative correlation of long chain *n*-alkanes C_{25} – C_{33} and TOC in the transitional unit and white micrite (grey interval in Figure 2).

Figure DR1. Example of GC-MS chromatographs of a limestone sample surface cleaned. Samples were sonicated 3x for 15 min in a solvent mixture of dichloromethane (DCM) and methanol (MeOH), 9:1 vol./vol.).

(A)   Wash 1
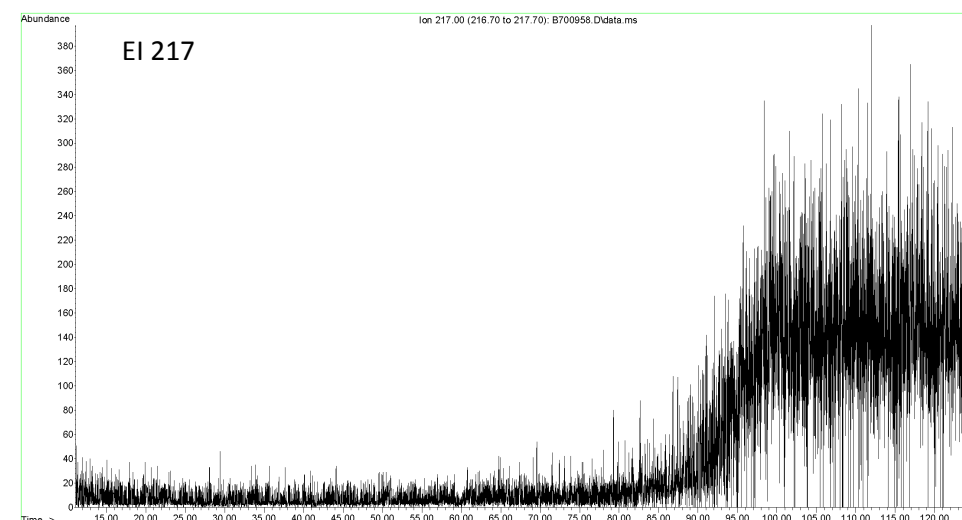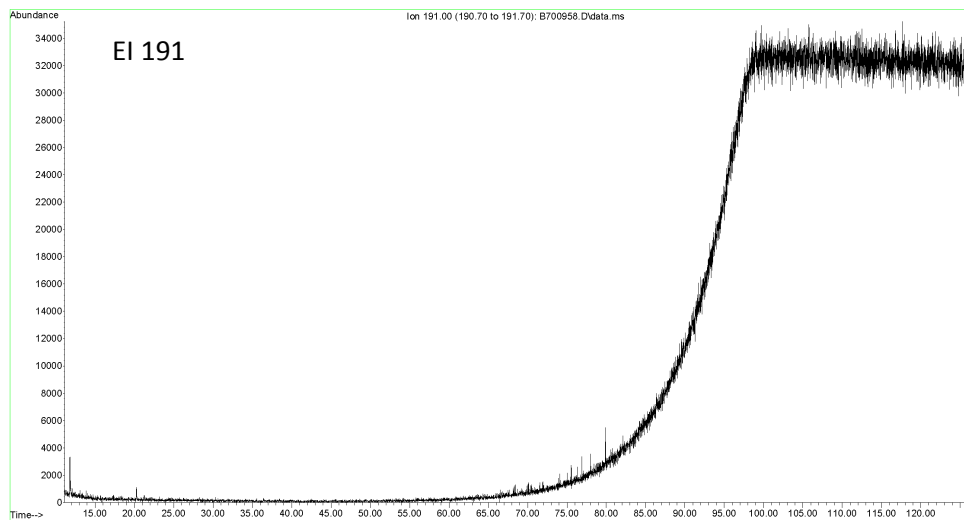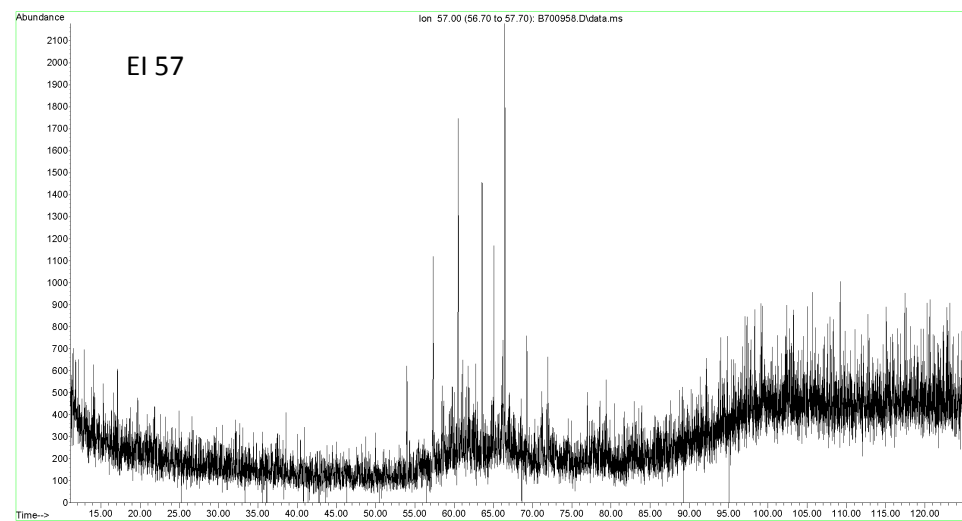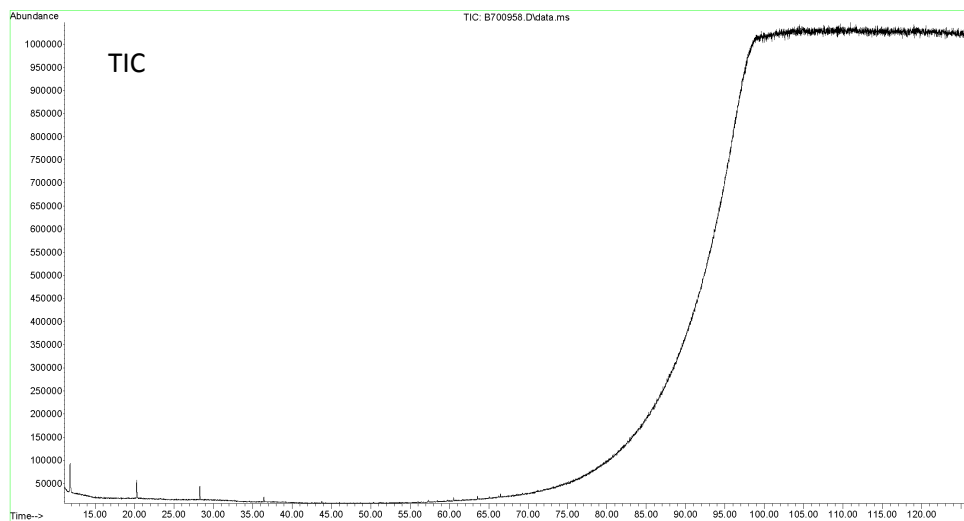(B)   Wash 2
(C)   Wash 3

Figure DR2. GC-MS chromatograms of a procedural blank. Empty thimble Soxhlet extracted 72 h using a solvent mixture of DCM:MeOH, 9:1 (vol./vol.).
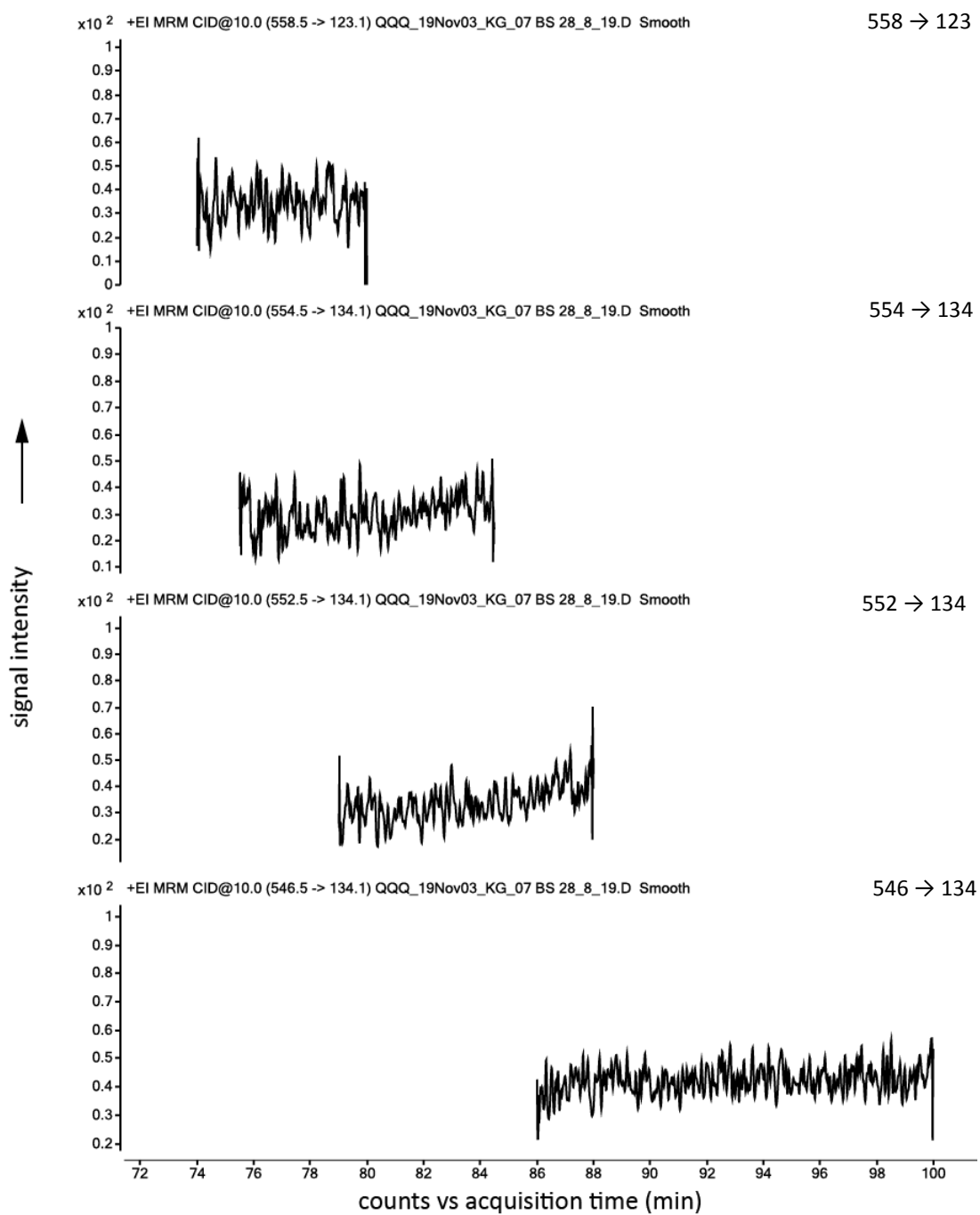
Figure DR3. MRM chromatograms of procedural blank (showing for carotenoids).
Empty thimble Soxhlet extracted for 72 h using a solvent mixture of DCM:MeOH, 9:1
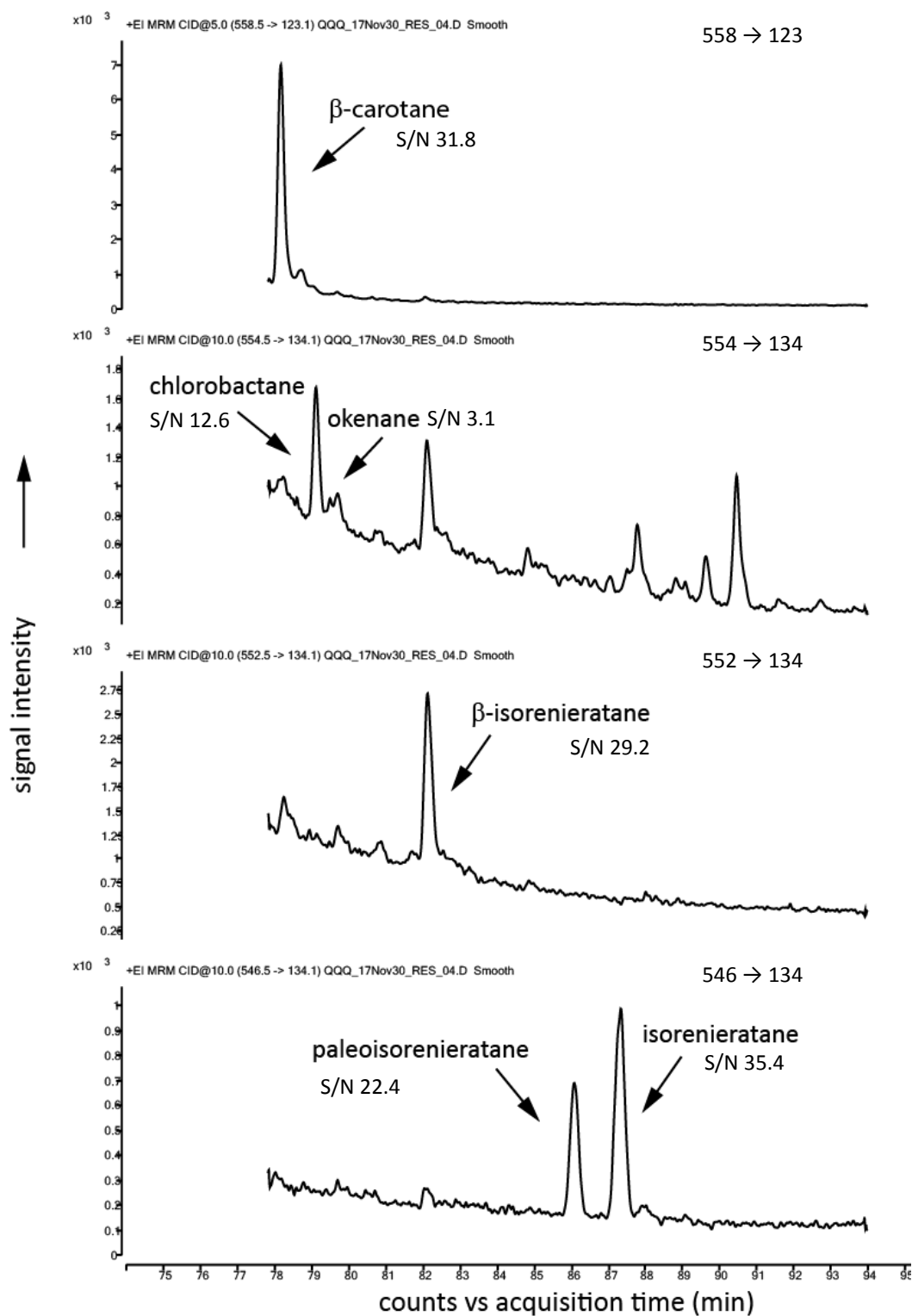(vol./vol.).3

Figure DR4. MRM-Chromatograms for carotenoids in a sample of the limestone interval at the depth of 613.12 mbsf. S/N: signal to noise ratio.
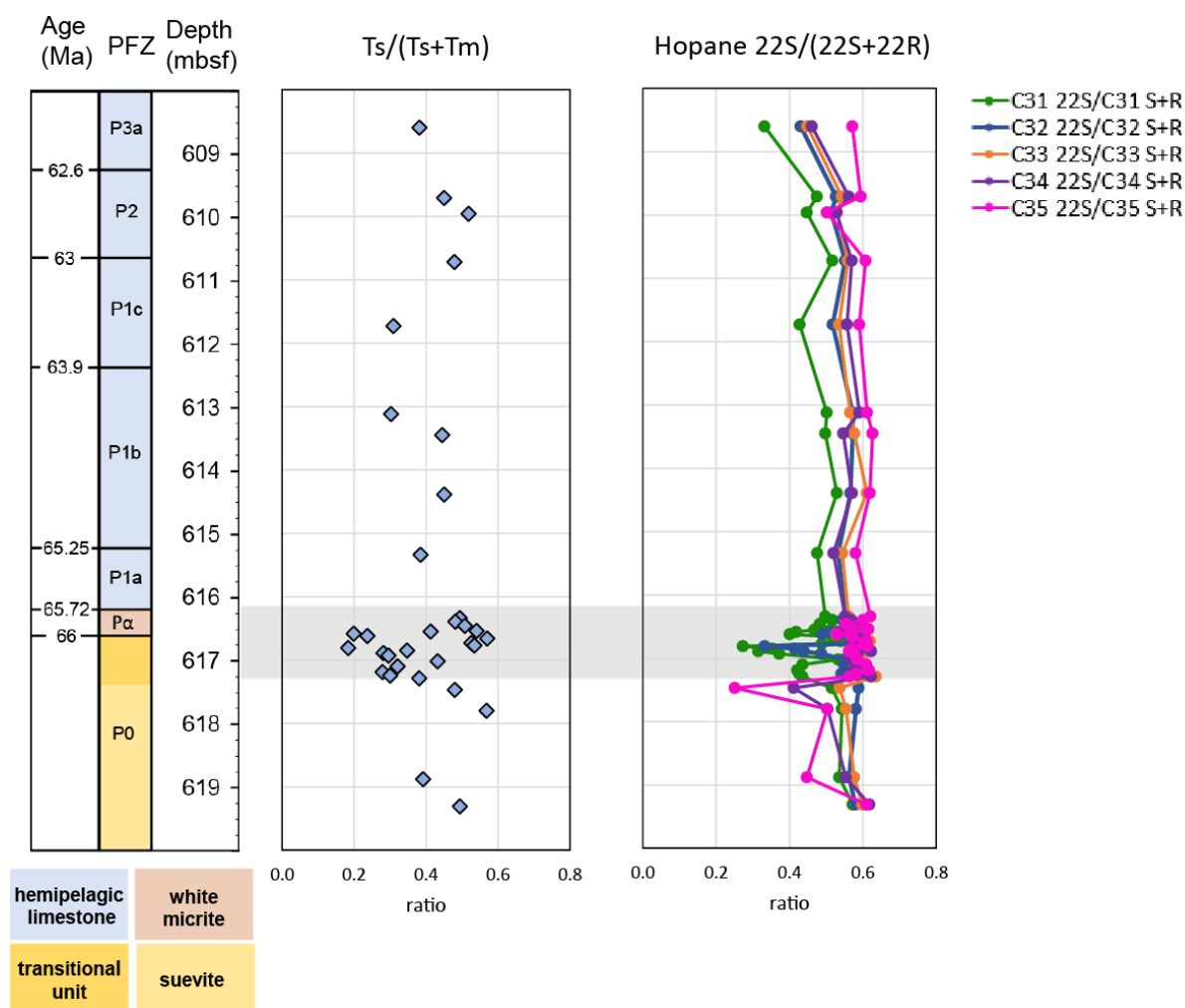
Figure DR5. Ts/(Ts+Tm) and homophopane 22S/(22S + 22R) ratios.
The ratios are 0.6 or below supporting low thermal maturity (Peters and Moldowan, 1991).
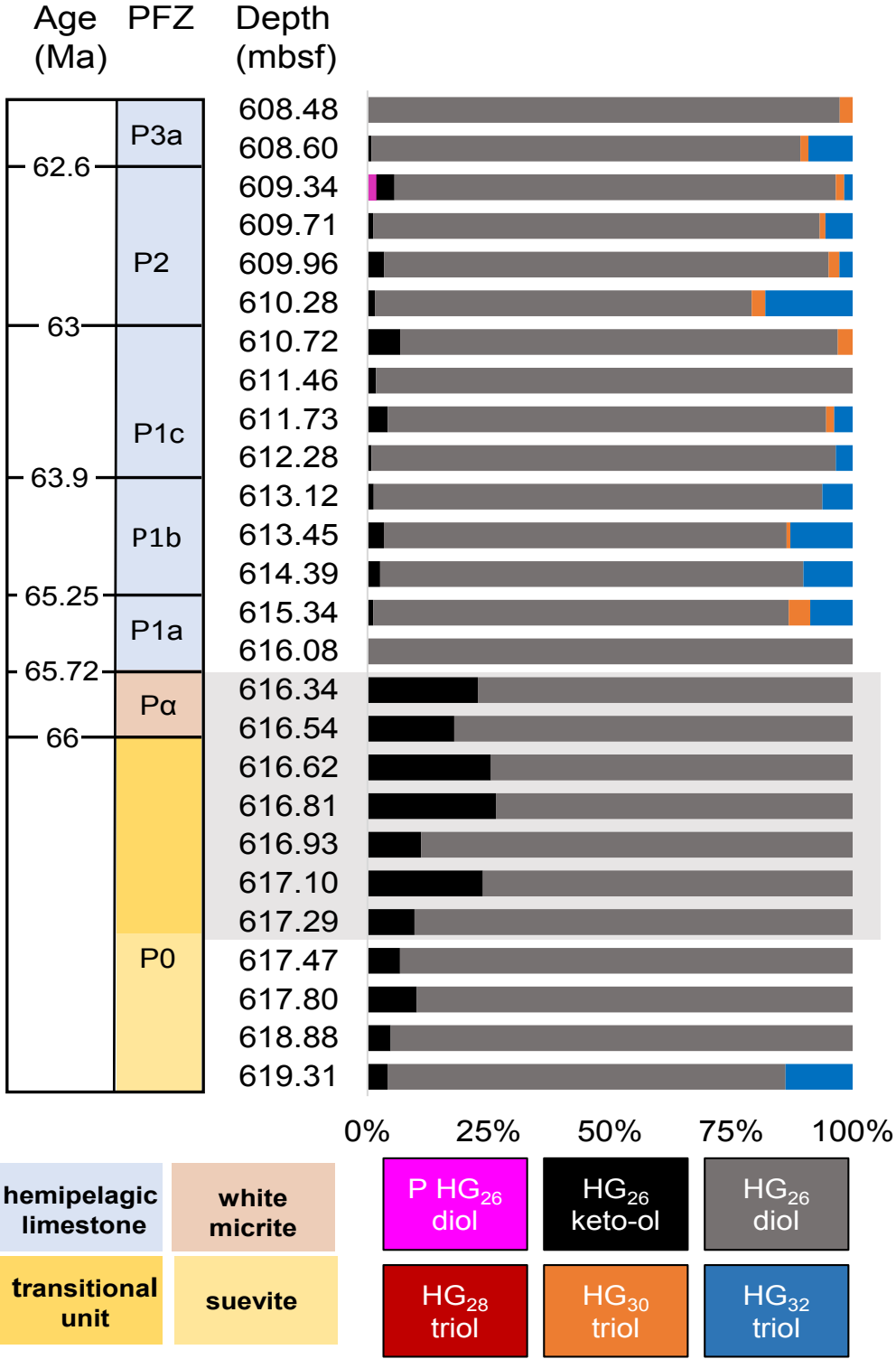(Ts (18α-22, 29, 30-trisnorneohopane), Tm (17α-22, 29, 30-trisnorhopane).

Figure DR6. Fractional abundance of heterocyst glycolipids (HGs). Fractional abundance of HGs derived from N2-fixing filamentous heterocysts in extractable lipids against the lithology of the Chicxulub core (Yucatán Peninsula, México) from IODP Site M0077. HG26 diol and keto-ol are the most commonly HGs found in the post-impact sediments only in the limestone interval HG30 and HG32 triol occur, indicating a shift in the cyanobacterial community. Compounds were identified by mass spectral characteristics (see supplementary text for analyses).
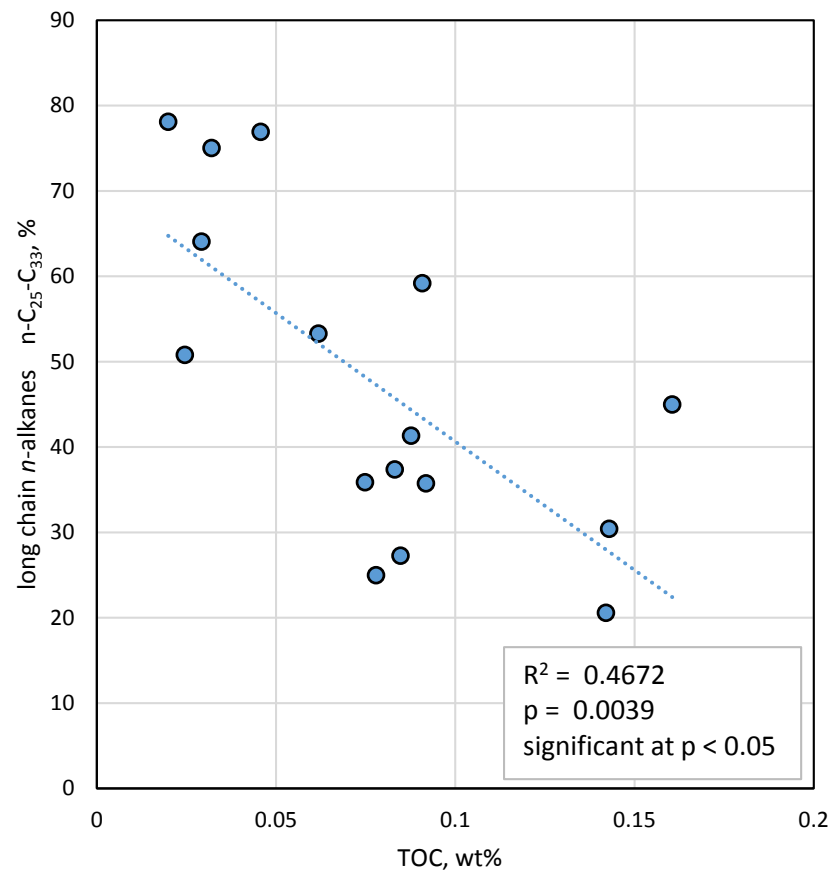
Figure DR7. Long chain n-alkanes C25 – C33 vs TOC.
Significant negative correlation of long chain n-alkanes
C25 – C33 and TOC in the transitional unit and white
micrite (grey interval in Figure 2).